THE ASTROPHYSICAL JOURNAL, 471:783–795, 1996 November 10

ALL-SKY SEARCH FOR TRANSIENT SOURCES NEAR 0.5 MeV WITH THE BURST AND TRANSIENT SOURCE EXPERIMENT (BATSE)

D. M. SMITH, M. LEVENTHAL, AND R. CAVALLO
Department of Astronomy, University of Maryland, College Park, MD 20742
N. GEHRELS AND J. TUELLER
NASA Goddard Space Flight Center, Greenbelt, MD 20771
AND
G. FISHMAN
NASA Marshall Space Flight Center, ES-62, Huntsville, AL 35812
Received 1995 December 8; accepted 1996 June 13

ABSTRACT

We present a search for bright, transient emission lines near 0.5 MeV in nearly two years of data from the Burst and Transient Source Experiment (BATSE) on the *Compton Gamma-Ray Observatory*. Such features have been reported from black hole candidates Nova Muscae and 1E 1740.7−2942 and from the Crab, lasting for ≈1 day. Our survey covers the whole sky and is sensitive to events with durations from 0.5–3.0 day. No transients are observed, and the systematic errors are low enough that the upper limits are significantly below the fluxes of the two most significant events previously reported.

Subject headings: Galaxy: center — gamma rays: bursts — gamma rays: observations — line: identification — surveys

1. INTRODUCTION

Positron-annihilation emission at 511 keV from the Galactic center region has been studied for the past 20 years. There is a long-standing debate as to whether this line is variable (see Lingenfelter & Ramaty 1989 for a historical review). The most recent observations, which are also the most sensitive (Share et al. 1990; Purcell et al. 1993; Smith et al. 1993; Gehrels et al. 1991; Leventhal et al. 1993), have shown no variability. But the observation from several Galactic sources of bright, short-lived transient emission features consistent with annihilation radiation has revitalized the idea of variability. In some cases, these features must be allowed to be redshifted and/or broadened to be consistent with annihilation. Since these transients are much brighter and much shorter lived than the historical variations of the Galactic center line, they are at most indirectly responsible for those variations, as discussed below.

Table 1 shows these recent transients. Most were observed with the SIGMA hard–X-ray imager on the *Granat* spacecraft, and one, from an unidentified source, was observed with the Medium Energy Detectors on *HEAO 1* (Briggs et al. 1995). The SIGMA transients are associated with the Crab and two black hole candidates: 1E 1740.7−2942 near the Galactic center and the X-ray transient Nova Muscae. There is also a long history of sporadic observations of lines near 75 and 400 keV from the Crab with balloon flights (see Owens 1991 or Harris, Share, & Leising 1994a for a summary).

The transients from black hole candidates have generated the most recent interest. The black hole candidacy of 1E 1740.7−2942 is based mostly on its hard X-ray spectrum, which is extremely similar to that of Cygnus X-1 in both its spectral shape and absolute luminosity (Heindl et al. 1993; Sunyaev et al. 1991). No companion has been identified, nor has a mass function been calculated, because of the optical extinction toward its position near the Galactic center. Only O stars and red supergiants can be ruled out as companions (Chen, Gehrels, & Leventhal 1994).

Several characteristics of 1E 1740.7−2942 make it particularly appealing as the source of a variable component to the Galactic center 511 keV line. It has a core-and-jet structure in the radio (Heindl et al. 1994; Mirabel et al. 1992; Rodriguez et al. 1992), and the high radio brightness of the jets, combined with their limited penetration into the ISM, implies that they are dominated by an electron-positron plasma (Chen et al. 1994). It is coincident in position with a molecular cloud (Bally & Leventhal 1991; Mirabel et al. 1991), which could be a site for subsequent cooling and annihilation of positrons escaping via the jets (Ramaty et al. 1992). Finally, a recent scan of the inner few degrees of Galactic longitude using the Oriented Scintillation Spectrometer Experiment (OSSE) on the *Compton Gamma-Ray Observatory* (*CGRO*) has shown that the peak of Galactic 511 keV emission is more consistent with the position of 1E 1740.7−2942 than with the Galactic center, about 1° away (Tueller et al. 1996).

Three of the transients in Table 1 are from 1E 1740.7−2942 and have been interpreted in several ways. Some positrons, created in a thermal pair plasma during an episode of high accretion, could annihilate in the accretion disk (Hua & Lingenfelter 1993), creating the broad, redshifted, immediate feature, while others escape via the jets to annihilate later in the molecular cloud or the ISM in general. Alternately, some could annihilate immediately near the base of the jets (Misra & Melia 1993; Maciołek-Niedźwiecki & Zdziarski 1994). Finally, the transient line-like emission features could even be created without annihilation by the Compton scattering of MeV continuum photons from slightly relativistic electrons in the jets (Skibo, Dermer, & Ramaty 1994).

One of the events in Table 1 is from Nova Muscae, one of a class of X-ray novae occurring about once per year in the sky. It showed characteristics typical of these objects: a sudden onset, exponential decay with constant on the order of tens of days, an X-ray spectrum with soft thermal and hard nonthermal components, a mass function indicating a

TABLE 1

REPORTED BRIGHT ~0.5 MeV TRANSIENTS

Source	Date	Duration[a]	Flux (photons s^{-1} cm^{-2})	Line Center (keV)	Line FWHM (keV)
1E 1740.7−2942[b]	1990 Oct 13–14	~1 dy	$(6.2 \pm 1.6) \times 10^{-3}$	385^{+30}_{-25}	110^{+60}_{-40}
1E 1740.7−2942[b]	1991 Oct 1–19	~18 dy	$(3.4 \pm 1.1) \times 10^{-3}$	380 ± 70	340^{+160}_{-90}
1E 1740.7−2942[c]	1992 Sep 19–20	1.16 dy	$(4.28^{+2.70}_{-1.50}) \times 10^{-3}$	350^{+110}_{-40}	170^{+210}_{-65}
Crab[b]	1992 Mar 10–11	0.95 dy	$(5.1 \pm 1.7) \times 10^{-3}$	536^{+11}_{-14}	44^{+41}_{-44}
Nova Muscae 1991[d]	1991 Jan 20–21	13 hr	$(6.3 \pm 1.5) \times 10^{-3}$	476 ± 15	58 ± 34
Unidentified[e]	Late 1977	~15 dy	$(6.0 \pm 1.0) \times 10^{-3}$	457 ± 16	213 ± 37

[a] Duration of the observation; in each case the event may have lasted longer. See the references for duration constraints.
[b] Gilfanov et al. 1994.
[c] Cordier et al. 1993.
[d] Sunyaev et al. 1992.
[e] Briggs et al. 1995.

black hole primary, and a weak secondary peak long after the primary outburst (Lund 1993; Orosz et al. 1994; Gilfanov et al. 1993). This class of object may have much in common with 1E 1740.7−2942 and other black hole candidates which are persistent emitters. There are a number of objects (e.g., GRS 1915+105, GRO J1655−40, GX 339) which show intermediate behavior over long timescales: neither a single, well-defined outburst like the X-ray novae, nor long-term, gradual variation in intensity like 1E 1740.7−2942, but rather multiple, irregular outbursts and long periods of dormancy. Furthermore, GRS 1915+105 and GRO J1655−40 both show relativistic radio jets with individual radio spots associated with particular X-ray outbursts (Mirabel & Rodriguez 1994; Hjellming & Rupen 1995).

Three of the transients in Table 1 occurred after the launch of *CGRO*. Data simultaneous with the 1992 transient from 1E 1740.7−2942 were available from OSSE and the Burst and Transient Source Experiment (BATSE). Both instruments set limits on such a transient inconsistent with the SIGMA best-fit Gaussian: a 3 σ upper limit of 1.0×10^{-3} photons s^{-1} cm^{-2} from OSSE (Jung et al. 1995) and a 3 σ upper limit of 1.8×10^{-3} photons s^{-1} cm^{-2} from BATSE (Smith et al. 1996). The BATSE 3 σ limit for the SIGMA Crab transient was 1.7×10^{-3} photons s^{-1} cm^{-2}. Wallyn et al. (1996), using the enhanced BATSE occultation package (EBOP), searched for the longer lived but fainter 1E 1740.7−2942 transient of 1991 and found a flux from 300–600 keV of $(1.43 \pm 3.05) \times 10^{-3}$ photons s^{-1} cm^{-2}, consistent with the both the SIGMA result and zero. The BATSE analysis technique described in this work and in Smith et al. (1996) is not suitable for such long-lived events.

The three most statistically significant events in Table 1, however, occurred at times when there was no second spacecraft to confirm or challenge the results. Therefore, any confirmation of these results will have to come from a statistical approach: long-term monitoring of these and similar sources to search for similar events.

A substantial effort in this direction has already been made using data from the *Solar Maximum Mission* Gamma-Ray Spectrometer (*SMM*/GRS) (Harris, Share, & Leising 1994a, 1994b). The *SMM* data run from 1981 to 1988, with each source visible for about 150 day yr^{-1} as the instrument's field of view moves along the ecliptic with the Sun. No events like the SIGMA Crab transient were reported, with an average 3 σ upper limit for a 1 day event of 2.92×10^{-3} photons s^{-1} cm^{-2}. No obvious candidates for flares like the 1990 1E 1740.7−2942 event were reported either. There were a few days with comparable fluxes, but no more than were consistent with the authors' expectations due to statistical and systematic errors: the average daily 3 σ upper limit was 4.84×10^{-3} photons s^{-1} cm^{-2}.

Below, we present a similar search using BATSE data. Although our analysis to date only spans 2 yr, we can examine the entire sky on each day, and the daily sensitivity is better than the *SMM*/GRS search due to the larger collecting area of BATSE. We will monitor later BATSE data as the *CGRO* mission continues.

2. INSTRUMENT, OBSERVATIONS, AND DATA ANALYSIS

2.1. *The Instrument and Data Formats*

BATSE (Fishman et al. 1989) is a set of eight modules, one on each corner of the *CGRO* spacecraft facing out from the center. Each uncollimated module has two Na I scintillators for hard X-ray and gamma-ray detection: a large area detector (LAD) of 2025 cm^2 and 1.27 cm thickness, and a spectroscopy detector (SD) of 127 cm^2 and 7.42 cm thickness. The SDs have good energy resolution and adjustable gain; some can be optimized for hard X-rays (10 keV–1 MeV), while others are set for gamma rays (less than 1 MeV to tens of MeV). The LADs have a fixed gain, with a useful energy range of approximately 30–1.7 MeV, and somewhat worse energy resolution. They are covered by a charged-particle detector (CPD) made of 0.64 cm of plastic scintillator for anticoincidence.

Our data are 5–10 minutes spectral accumulations with the finest energy binning available from BATSE (i.e., the HER_COR and SHER_COR formats for the LADs and SDs, respectively). When we calculate parameters which predict the background (see below), we use the time of the midpoint of each spectral accumulation since with an orbital period of about 90 minutes there can be significant background variation in 5 minutes. Another data format (DISCLA) is used to obtain the spacecraft position and the rates in the CPDs.

2.2. *Background Selection*

As a large-area, uncollimated array of detectors, BATSE was optimized to observe bright, short-lived events like gamma-ray bursts and solar flares. For these events, the source count rate can dominate the background, and even when it does not, the background can be easily determined by averaging data just before and after the event.

For longer observations, the background must be modeled and subtracted in a more sophisticated way. The cosmic diffuse sky, the Earth's atmosphere, and activation of the spacecraft and the detectors themselves by cosmic rays and trapped particles in the South Atlantic Anomaly (SAA) all contribute to the background. We are developing a number of methods of background subtraction, but two are used for the work presented here: background selection by one-day offset, and background selection by parameter matching. Both techniques involve the selection, for each source spectrum, of one or more spectra which should have the same background level but which either (1) occur outside the time we are testing for transient flux or (2) do not have the object we are testing in the detector's field of view. Since the transients of Table 1 are much brighter than any object in the sky in their energy range, we are not concerned with other sources in the field of view.

The background-subtraction techniques are described in detail in the Appendix and are similar to those used by Harris, Share, & Leising (1994a, 1994b) for *SMM*/GRS.

When we are looking for an event of duration ≤ 1 day, we select background by one-day offset: we examine the spectra exactly 15 orbits (about 1 day) before and after the source spectrum, and, if they are suitable for use, we average them to use as the background. If only one of the two days is suitable, that one is used, although we achieve better background subtraction when we can use both since long-term variability in the background then averages out. If neither background spectrum is suitable, the source spectrum is discarded. The parameters used to evaluate the suitability of a background spectrum are discussed in the Appendix.

When searching for a transient which lasts more than a day, we can no longer use a one-day (15 orbit) offset to find a background spectrum which we know will match well in most parameters. We instead find a background spectrum by parameter-matching: we consider every spectrum which is within the same pointing period of *CGRO* as the source spectrum (usually a period of 1–3 weeks) but which does not include the transient we are testing for. We find the spectrum which minimizes a weighted sum of the differences in all of the parameters between source and background. Once this background spectrum is chosen, the procedure is the same as for the one-day–offset analysis.

2.3. *Background Adjustment*

Despite the careful choice of background spectra, there are still residual variations high enough to produce systematic errors of the order of the signals we are looking for. The transients in Table 1, although very bright by the standards of gamma-ray line astronomy, have fluxes on the order of 2% of the LAD background at their peak; we must therefore subtract background over the course of a day to much better than 2%.

We therefore make three adjustments to the background spectra once they are chosen. We add or subtract small multiples of prototypical spectra we call "templates." Each template corresponds to a particular parameter. It is generated by subtracting thousands of source/background spectral pairs matched using the same rules as when looking at a particular cosmic source. We then look at the average spectral difference as a function of the difference in the parameter of interest. We generate three types of template, which are optimized for different purposes; they are described in detail in the Appendix.

The amount of each template added is a function only of the values of the parameters; at no time do we fit the spectrum using the templates or, indeed, consider the source spectrum below 1 MeV in any way during the background subtraction. Thus, we believe the final result to be free of any biases toward null results. Although the background subtraction algorithm was, of course, created by trying many types of analysis and finding the one which produced the smallest differences between source and background, these comparisons were always made using hundreds of days of data either uniformly spread over the sky or else concentrated at the Galactic poles where no sources are expected. In this way, the existence of a few real transients would not affect the way the analysis evolved.

2.4. *Line Fitting*

The search for line transients in background-subtracted data is performed using Monte Carlo simulations of BATSE's response to line transients at various energies. We test for eight Gaussian lines, which are listed in Table 2. We simulated the response of the LADs and SDs to each of these lines, at incident angles to the detector axis from 0° to 80° in 10° increments. These simulations include the effects of partial energy deposits in the detectors, scattering from the spacecraft, and energy resolution. Using the data from one period (0.5–3.0 day) and from one detector we interpolate between the simulations based on the exact incident angle. Then, for each line, we fitted the simulation to the observed spectrum, using all data which fall within twice the FWHM of the line center but above 300 keV. The best-fit simulated flux and its 1 σ error are recorded as the result of that detector for that line during that period.

For each period, the results of multiple detectors are added, weighted by the inverse square of the errors in the fits. At least two and usually three LADs are available for every period. Because of the widely varying gains of the SDs and spectral artifacts which appear in the high channels of

TABLE 2

TRANSIENT LINES SEARCHED FOR IN THE ALL-SKY ANALYSIS

Center Energy (keV)	FWHM (keV)	FWHM Including LAD Resolution	Explanation
350	170	187	1992 1E 1740.7−2942 transient (Cordier et al. 1993)
385	110	137	1990 1E 1740.7−2942 transient (Gilfanov et al. 1994)
420	0	88	Narrow annihilation line on NS surface
436	200	219	Thermally broadened annihilation line on NS surface
476	58	112	SIGMA Nova Muscae transient (Sunyaev et al. 1992)
511	0	102	Narrow annihilation line
531	200	225	Thermally broadened annihilation line
536	44	114	SIGMA Crab transient (Gilfanov et al. 1994)

some of them, there are often only one or two available.

2.5. *The Observations*

We have tried to make our analysis flexible enough to catch bright transients over a large range of the relevant parameter space: position on the sky, time of occurrence, duration, center energy, and energy width. Any line with its center from just below 350 keV to just above 536 keV and with a FWHM from 0 to 200 keV will coincide closely enough with at least one of the lines in Table 2 to appear with the better part of its true flux.

To cover the whole sky, we analyze a grid of 26 positions: the north and south Galactic poles, and points spaced by 45° in Galactic longitude at Galactic latitudes 0° and ±45°. Any point in the sky is then no farther than 22°.5 from the nearest grid point. A sampling of random points on the sky shows that at least 85% and usually closer to 95% of the data used at the grid point nearest to a random point would include a source at that random point. Thus, any source will appear with at least 85% of its flux at some grid point.

To achieve the best coverage of timing consistent with the limitations of our background-subtraction methods, we begin by analyzing all grid points at all energies in 0.5 day intervals. In addition to analyzing these intervals for short transients, we can also sum them together in pairs to search for 1 day transients. By summing them two ways, beginning with the first 0.5 day interval and beginning with the second, we can be sure to catch any event which, in one of the summations, might have straddled a day boundary, thereby appearing in both source and background spectra and partially subtracting itself out.

More than two 0.5 day intervals may not be summed because their background spectra were selected by 1 day offset. To search for events up to 3 days in duration, we use 3 day intervals with the background selected by parameter-matching. To avoid missing an event because it straddles the boundary of two 3 day intervals, we ran the 3 day analysis 3 times, grouping the days starting with the first, second, and third day of available data.

3. RESULTS

The total data set resulting from the search consists of 1248 time series of line fluxes: eight lines (see Table 2) at 26 sky points sampled at six time intervals (0.5 days, 1 day with two starting points, 3 days with three starting points). Each time series contains between 250 and 1400 points depending on the interval length. It is impractical to present all these data here, but we will present some sample plots of particular interest and a summary of the entire survey.

Figure 1*a* shows a 1 day count spectrum for the three LADs nearest the north Galactic pole on a day with a typical (1 σ) residual background. The dotted curves shown along with it are the simulated detector response to the eight lines of Table 2, each with a flux of 5×10^{-3} photons s^{-1} cm^{-2}. The negative curve is 2% of the total subtracted background. The rms residual background for 1 day spectra is 0.15% of the total background, using two or three detectors (depending on the spacecraft orientation). Figure 1*b* shows the same day in one of the SDs (only one SD was usable on this day for this direction in the sky).

3.1. *Transients from 1E 1740.7−2942*

Figure 2 is one data set of particular interest: a line like the 1990 October transient of 1E 1740.7−2942 (Table 2, line 2) using the ($b = 0°$, $l = 0°$) grid point, which is only 1°

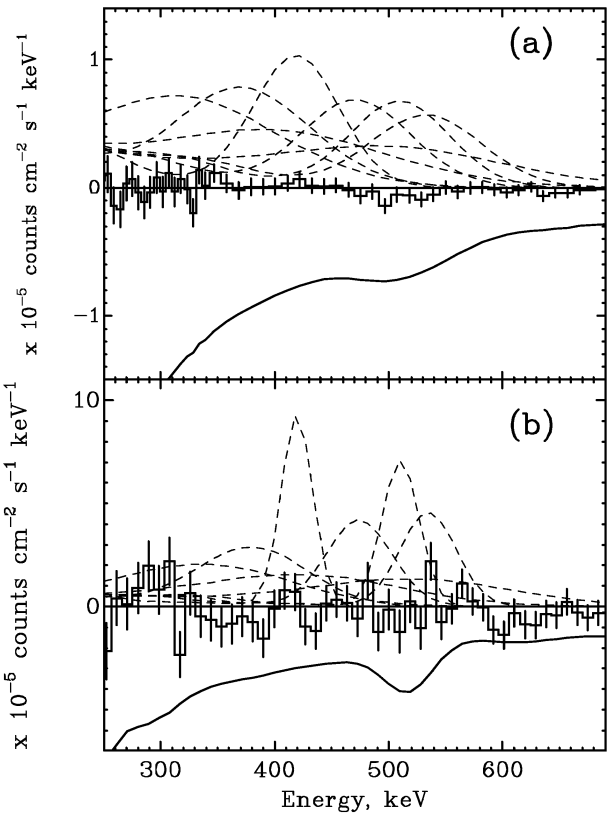

FIG. 1.—Typical daily background-subtracted spectra (with statistical error bars) in three LADs (*a*) and one SD (*b*). The negative trace in each plot is 2% of the background. The dotted traces are the eight lines of Table 2, each given a flux of 5×10^{-3} photons s^{-1} cm^{-2} (typical of the events in Table 1) and convolved with the detector responses.

from that source. The top plot is for the LADs and includes both sets of 1 day intervals: that beginning at 0 hr UT each day and that beginning at 12 hr UT. The following plots are for 0.5 day intervals in the LADs, for 3 day intervals in the LADs using all three sets of points beginning on different days and for 1 day intervals in the SDs. The error bars shown are statistical; it is clear that the systematic errors are somewhat higher. Shown alongside the time series is a histogram of the values in the series. The distributions are nearly Gaussian; for the 1 day intervals, the 1 σ width of the best fit Gaussian is 0.48×10^{-3} photons cm^{-2} s^{-1}.

For the data beginning at 0 hr UT each day, there are a total of 665 days shown in the span of 918 days from 1991 June 9 (TJD 8410) to 1993 December 6 (TJD 9327). The data fraction is similar for the points offset by 12 hr. Missing days are disqualified for one of three reasons: a *CGRO* repointing sometime during the day, less than 15,000 s total data among all usable LADs, or very high geomagnetic activity. Geomagnetic activity is measured by the standard global index A_p, which is considered too high if greater than 150 at any time during the source and background days or greater than 90 when averaged over the source and background days. There are several factors which each cause a fraction of the days to have higher systematic errors than the majority and which include the following:

1. *One-sided background.*—For the 0.5 day and 1 day time series, some days can only use one day (either before or after) for background because the other day contains a

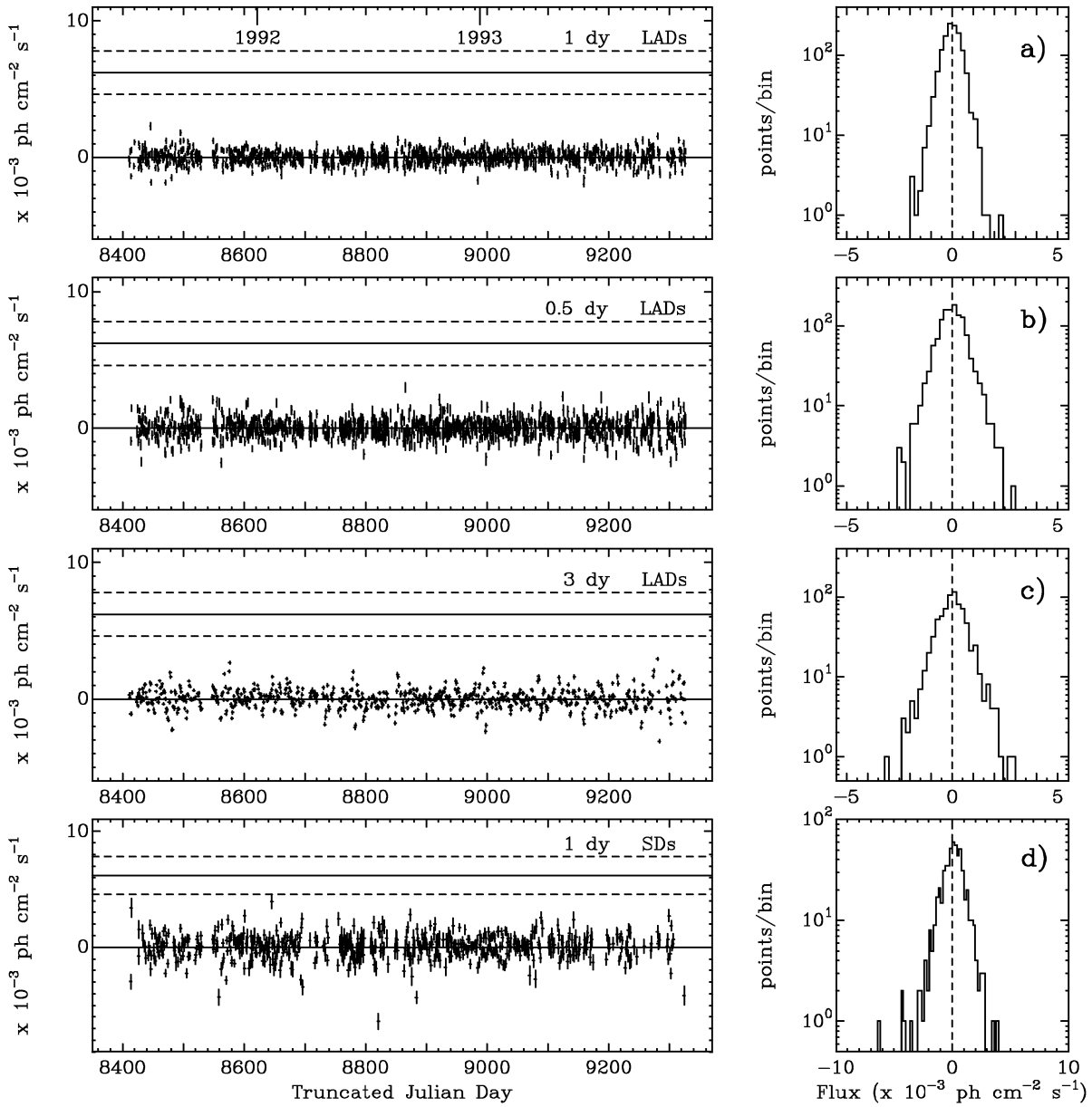

FIG. 2.—Search for a transient from 1E 1740.7−2942 like the 1990 event. *Left:* time series of line fluxes. *Right:* histograms of the points in each series in bins of width 0.2 × 10^{-3} photons s^{-1} cm^{-2}. (*a*) 1 day intervals, series starting at 0 hr UT and 12 hr UT; (*b*) 0.5 day intervals; (*c*) 3 day intervals, series starting on the first, second, and third days of data; (*d*) 1 day intervals in the SDs, series starting at 0 hr UT only. The flux and 1 σ errors for the 1990 event are shown for comparison.

CGRO repointing. Since long-term background variations are not averaged out, the rms of these points is higher.

2. *Higher than average rate of orbital change.*—When the spacecraft is undergoing a reboost the orbital parameters vary much more rapidly from day to day. The variation among these days is higher than among days when the orbit varies little.

3. *Higher than average geomagnetic activity.*—In the crudest approximation, periods of high A_p are rare events which last $\lesssim 1$ day and which result in a lowering of the BATSE background. Not only does this create a subset of points with a larger-than-average error, but this subset is asymmetrical: the day with high A_p can have a very negative background-subtracted flux, but the days which use that day as background will have only somewhat positive fluxes since in general they will have one or more other days they are also using for background. We do not use a template correction in the A_p parameter for two reasons: because the extent of the depression of the background can vary widely for the same value of A_p and because some of the correction is done automatically by the existing template which uses the count rate greater than 1 MeV (see Appendix).

4. *Lower than average integration time.*—Data for a given day summed over up to three detectors can vary from 15,000 to ~100,000 s. The systematic errors tend to decrease as more data are used, although not in the predictable way statistical errors do.

It would be possible to eliminate all days which are subject to one or more of these effects, but this would result in losing about half the data in Figure 2. Instead we have eliminated (as mentioned above) only the most extreme

cases of the last two problems: high A_p and sparse data. Within the data we kept, we measured the effect of these four sources of error on the 1 day rms line flux in a single detector facing the north Galactic pole, using the line parameters of the 1990 1E 1740.7−2942 transient. The days with good integration time, background both before and after, low A_p, and little orbital change had an rms scatter of 0.4×10^{-3} photons s^{-1} cm^{-2}. The average rms of days with one-sided background was 0.7×10^{-3} photons s^{-1} cm^{-2}. The days with the lowest accepted integration times, those with the highest accepted values of A_p, and those with the largest orbital derivatives all gave rms values around 0.9×10^{-3} photons s^{-1} cm^{-2}.

Also shown in Figure 2 are plots for 0.5 day intervals (*b*), 3 day intervals with all three offsets shown (*c*), and 1 day intervals using the SDs, with only the set starting at 0 hr UT shown (*d*). It is obvious that the SDs have both greater statistical and systematic errors than the LADs. This is even more true for the broadest of the lines in Table 2, as is apparent from looking at Figure 1*b*. The SDs are also more difficult to analyze on a large-scale basis for two reasons: the varying gains require frequent operator verification of the results of automated gain calculations, and the larger number of channels (256 vs. 128 for the LADs) increases the time required for rebinning, subtracting, and fitting spectra. We have therefore not pursued the use of the SDs beyond the production of this one time-series and the analysis of data for two of the SIGMA transients presented in Smith et al. (1996).

It is clear that no transient event approaching the flux reported by SIGMA in 1990 October from 1E 1740.7−2942 occurred in 665 days. The equivalent plots using the center energy and width of the 1992 September flare are similar. We can quantify the disagreement between our data set and SIGMA's by calculating the probability that both data sets sample the same frequency of transients and that these transients occur as a Poisson process, with a constant probability per unit time of a transient occurring. We define T_S and T_B as the total number of days observed by SIGMA and BATSE, respectively, H_S and H_B as the number of days that each instrument sees a transient occurring, and x as the true probability of a transient occurring on any given day. As of 1993 April, $T_S = 64$ and $H_S = 2$ (Cordier et al. 1994); from our data in Figure 2*a*, we have $T_B = 665$ and $H_B = 0$. If we ignore the possibility of false positives and false negatives from both instruments, then the probability that the SIGMA and BATSE data agree as to the duty cycle of occurrence is

$$P = \left[\sum_{i=0}^{H_B} \frac{T_B!}{(T_B - i)!\, i!} (1 - x)^{T_B - i} x^i\right] \times \left[1 - \sum_{i=0}^{H_S - 1} \frac{T_S!}{(T_S - i)!\, i!} (1 - x)^{T_S - i} x^i\right], \quad (1)$$

i.e., the probability of seeing H_S *or higher* while seeing H_B *or lower*. In this case the probability is maximized at 2.2×10^{-3} for a source-on duty cycle x of 2.8×10^{-3}. In other words, the level of disagreement between the two data sets may be as small as 3 σ, but only if the true frequency of occurrence is 14 times lower than the most probable value from the SIGMA data set alone (2/64). If the SIGMA frequency were correct, the probability of seeing no transients in 665 days with BATSE would be 6.8×10^{-10}.

We do not have enough information about the sensitivity of the full set of SIGMA observations to specify the probability of false positives and negatives in that data set. If the 1992 September event, which was not seen to high sensitivity by OSSE (Jung et al. 1995) and BATSE (Smith et al. 1996), is indeed a false positive then $H_S = 1$ and the joint probability is maximized at 3.4×10^{-2} for a duty cycle x of 1.5×10^{-3}.

The rate of false negatives in BATSE should be small due to the high sensitivity of the data. We can estimate it by assuming that the flux we are searching for is the lower of the two SIGMA events (4.28×10^{-3} photons cm^{-2} s^{-1}) and that the frequency of occurrence of such events is determined by the SIGMA rate of 2/64 days. Both of these assumptions are liberal in the sense of maximizing our rate of false negatives. Then we can sum, over all 665 days, the product of the probability that an event occurs on that day (2/64) and the probability that the low flux we recorded on that day really should have been 4.28×10^{-3} photons cm^{-2} s^{-1} but for an unlucky multiple of our empirical rms error. We find that the expected number of false negatives is then 2.5×10^{-9}.

3.2. *Transients from the Crab*

Although our previous paper (Smith et al. 1996) set a highly restrictive limit for the one Crab transient reported by SIGMA, we have searched specifically for this line among the full data set. Figure 3 shows this search in 0.5 days, 1 day, and 3 day intervals. The limits for a narrow line at 420 keV (approximately the redshift on a neutron star surface) are even stricter due to lower systematic errors, with no point higher than 2.3×10^{-3} photons cm^{-2} s^{-1} at any timescale.

There is a prominent pair of high and low points at TJD 9308 and 9309 (1993 November 17 and 18) in Figure 3*a*. This was an unusual two-day pointing period for *CGRO*, so each day is used as the background for the other, and this pattern is what would be expected if the first day had extra flux. We believe that this extra flux (which has a spectral shape consistent with a narrow 511 keV line) is background due to activation because it is seen *from all directions in the sky* and only during orbits following SAA passages, when short-lived activation of a 511 keV line is always seen. In general our third template correction, for activation at the 25 minutes half-life of ^{128}I (see Appendix), is supposed to compensate for just this excess. However, this pair of days is in a uniquely bad position for the reliability of this correction for three reasons: (1) it occurs during one of a few stretches of time (TJD 9300−9311) for which we have little OSSE data to give us SAA particle doses (see Appendix), (2) it occurs during the *only* stretch of time (TJD 9250−9315) in which, due to reboost maneuvers, *CGRO* is in an elliptical orbit with over three times its usual eccentricity (this results in a more variable background since the altitude at which the SAA is traversed varies from pass to pass), and (3) it is a one-sided background subtraction (see above), which aggravates the other uncertainties by not letting slow (more than 1 day) variations average out. This pair of days is not noticeable in the plot for 1E 1740.7−2942 because the data for that half of the sky are dominated by non-SAA orbits on day 9308.

3.3. *Transients from X-Ray Novae*

The Nova Muscae transient was seen by SIGMA 12 days after the discovery of the X-ray nova and about 6 days after

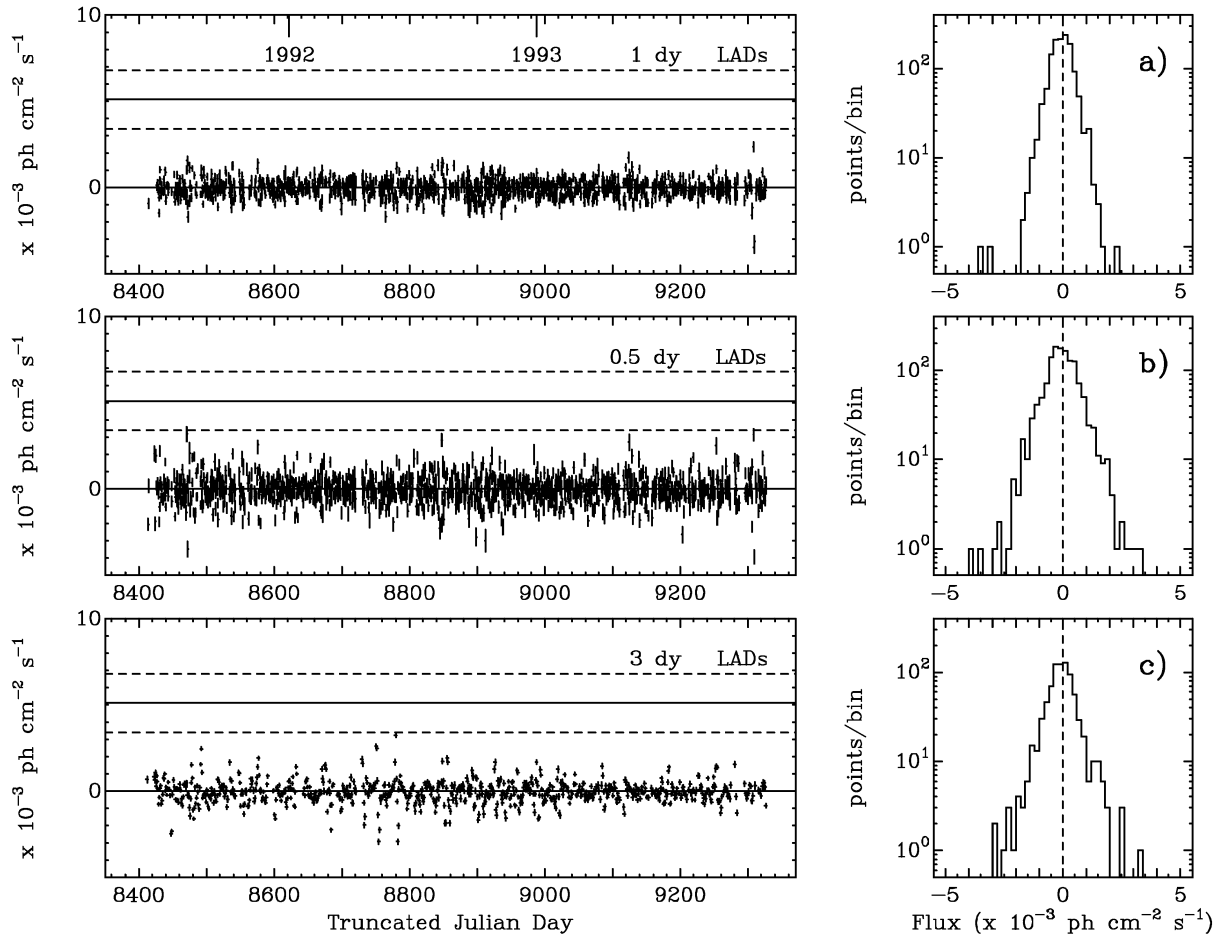

FIG. 3.—Search for a transient from the Crab like the SIGMA event. *Left:* time series of line fluxes. *Right:* histograms of the points in each series in bins of width 0.2×10^{-3} photons s^{-1} cm^{-2}. (*a*) 1 day intervals, series starting at 0 hr UT and 12 hr UT; (*b*) 0.5 day intervals; (*c*) 3 day intervals, series starting on the first, second, and third days of data. The flux and 1 σ errors for the SIGMA event are shown for comparison.

its maximum (Goldwurm et al. 1992). Four X-ray novae were observed through their peaks by BATSE during the period covered by this paper: 4U 1543−47, Nova Persei (GRO J0422+32), GRS 1009−45, and GRO J1719−24 (Harmon et al. 1994). Figure 4 shows 1 day fluxes for a Nova Muscae–type line (Table 2, fifth entry) from the sky point nearest each of these objects from 10 days before its initial outburst to 40 days after. Both sets of 1 day points are included on these plots: those beginning at 0 hr UT and those offset to begin at 12 hr UT. No flare events are seen, although there are data gaps due to either poor data coverage or *CGRO* repointings. The Nova Muscae flux is shown for comparison, but the comparison is not very meaningful; Nova Persei was considerably brighter than Nova Muscae and might be expected to have a brighter transient line if such were to occur, while the other X-ray novae were either comparable (GRO J1719−24) or dimmer in peak hard X-ray intensity.

3.4. *All-Sky Survey*

Figures 5–7 summarize the results for all 26 sky points. Each histogram is for a particular line from Table 2 and a particular interval duration but contains data from all available intervals and all sky points. Many of the points included in each histogram are not independent of each other for two reasons: in the 1 day and 3 day plots (Figs. 5 and 7) points taken with different time offsets overlap, and in all three plots simultaneous results from nearby sky points contain much of the same data.

There are 33,720 1 day trials for each line, counting all sky points and days and both offsets. As can be seen in Figure 5, not one of these trials reaches the corresponding line flux reported by SIGMA. The statistical analysis used specifically for 1E 1740.7−2942 above cannot be used here because T_B must be a number of *independent* trials.

Figure 6 shows histograms of the 34,893 0.5 day intervals in the all-sky survey. For the two brightest SIGMA lines (Nova Muscae and 1E 1740.7−2942 in 1990) there is again no interval which approaches the reported flux. The fluxes for the two dimmer transients (the Crab and 1E 1740.7−2942 in 1992) appear on the tails of the distributions. For the former, the reported flux of which was 5.1×10^{-3} photons cm^{-2} s^{-1}, there is one point at +4.9 and one at -4.9×10^{-3} photons cm^{-2} s^{-1} in our data. For the latter, there are six intervals higher than the SIGMA flux of 4.28×10^{-3} photons cm^{-2} s^{-1}, and 31 intervals lower than the opposite of that flux. This asymmetry can be attributed to the effect of geomagnetic disturbances, as described above. These two dimmer transients are, at any rate, the ones which were not seen at high sensitivity in contemporaneous observations (Jung et al. 1995; Smith et al. 1996).

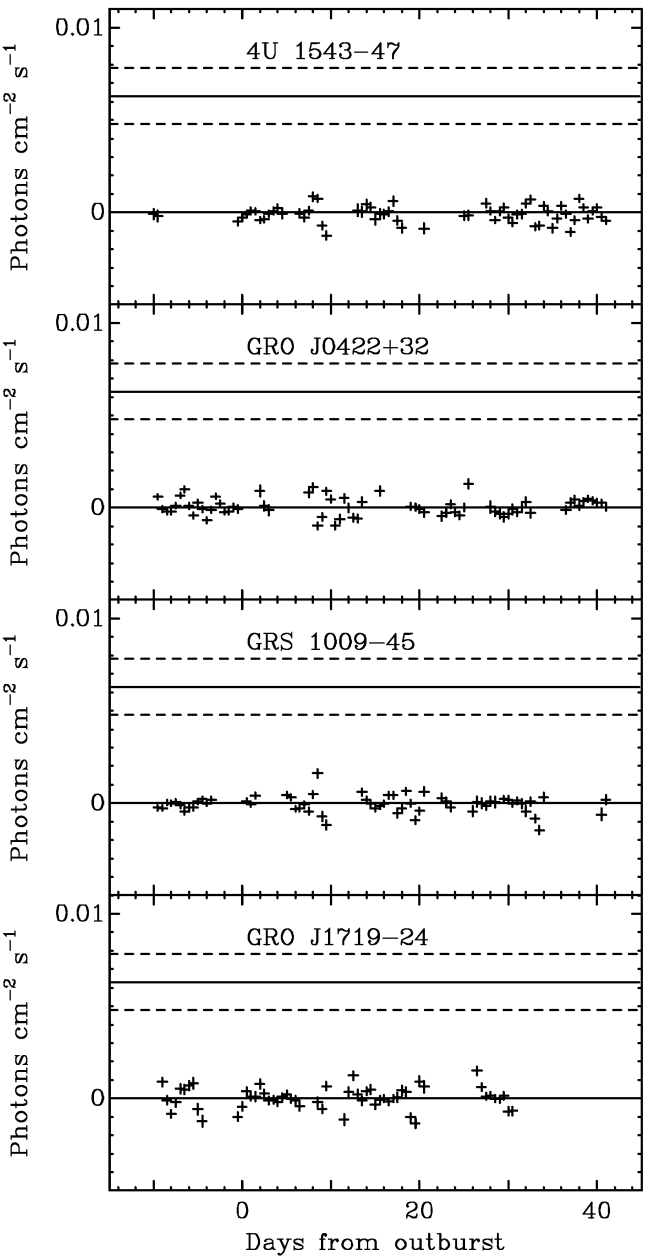

FIG. 4.—Search for 1 day transients like the Nova Muscae event from four X-ray novae. The flux and 1 σ error of the Nova Muscae event (which occurred at 12 days from outburst) are shown for comparison. Points starting at both 0 hr UT and 12 hr UT are shown.

TABLE 3

3 σ SENSITIVITIES VERSUS LINE ENERGY AND DURATION[a]

Energy (keV)	1 Day Sensitivity ($\times 10^{-3}$ photons cm^{-2} s^{-1})	0.5 Day Sensitivity	3 Day Sensitivity
350.....	1.85	2.66	2.44
385.....	1.46	2.10	1.90
420.....	1.00	1.44	1.24
436.....	2.08	3.01	2.71
476.....	1.37	2.01	1.72
511.....	1.43	2.10	1.75
531.....	2.26	3.30	2.84
536.....	1.46	2.15	1.73

[a] See Table 2 for line widths.

Finally, Figure 7 shows the 18,486 3 day intervals. The three brightest SIGMA transient fluxes are not approached by any of the points. There is one data point in the distribution for the 1992 line from 1E 1740.7−2942 (350 keV) with a flux equal to that reported by SIGMA, and two points with negative fluxes that exceed its magnitude. These three points are for the time intervals TJD 9304−9307 (positive point), 9301−9304 (most negative point), and 9302−9305 (penultimately negative point). These extreme values occur in circumstances almost identical to those which produced the extreme pair of points in the daily time history of the Crab (see Fig. 3*a*). The excess occurs, to a greater or lesser extent, over the whole sky. The dates are during the same, unique overlapping period of orbital eccentricity and lack of OSSE data on SAA particle doses. The background subtractions are primarily one-sided, since this *CGRO* pointing lasted from TJD 9301−9307. The difference between this case and the case of the Crab points is that the spectrum is dominated by a peak at 200 rather than 511 keV. From our template studies (see Appendix) we know that a 200 keV peak is characteristic of longer lived activation at the 15 hr half-life of ^{24}Na. And, indeed, in this case we see the spectral excess during all orbits, not just those with SAA transits.

Table 3 shows the 3 σ sensitivities to each line at each duration, derived by taking three times the rms value for each histogram.

4. CONCLUSION

We conclude that there is no evidence in BATSE data from 1991 June to 1993 December for transient emission lines from any part of the sky with durations from 0.5–3 days, at energies from 350–536 keV and above the flux levels in Table 3. These sensitivities are improved over those of SIGMA and *SMM*/GRS for comparable durations. The total data coverage is roughly 1 order of magnitude higher than SIGMA's for the Galactic center and presumably even higher for other parts of the sky, which were less frequently observed by SIGMA.

We can make no statement at this time about longer lived features (such as the dimmer, 18 day transient from 1E 1740.7−2942 in 1991; Churazov et al. 1993). We saw nothing like the Nova Muscae transient from four X-ray novae, but our data sets (Fig. 4) contain gaps, and there may be reasons why one such event (Nova Muscae) might produce a transient while others did not.

We thank the many people who have helped us acquire and process BATSE data, including Mark Finger, Brad Rubin, John Hladky, Michael Briggs, Mike McCollough, Charles Meegan, and others at NASA-Marshall Space Flight Center, and Chris Shrader, George Gliba, Nick Ruggiero and others in the *CGRO* Science Support Center (SSC) at NASA-Goddard Space Flight Center. We are grateful for useful conversations on the BATSE background with Jim Ling and Bill Wheaton of the Jet Propulsion Laboratory. Tom Bridgman of the SSC provided OSSE data on the radiation doses picked up by *CGRO* during SAA transits. We also thank Michael Harris and Gerald Share for valuable insights based on their similar analysis of *SMM*/GRS data. Finally, special thanks to Eric Chipman for setting up the earliest version of this analysis.

This research has made use of data obtained through the *CGRO* Science Support Center GOF account, provided by the NASA-Goddard Space Flight Center. It was supported in part by NASA grant NAG 5-2380.

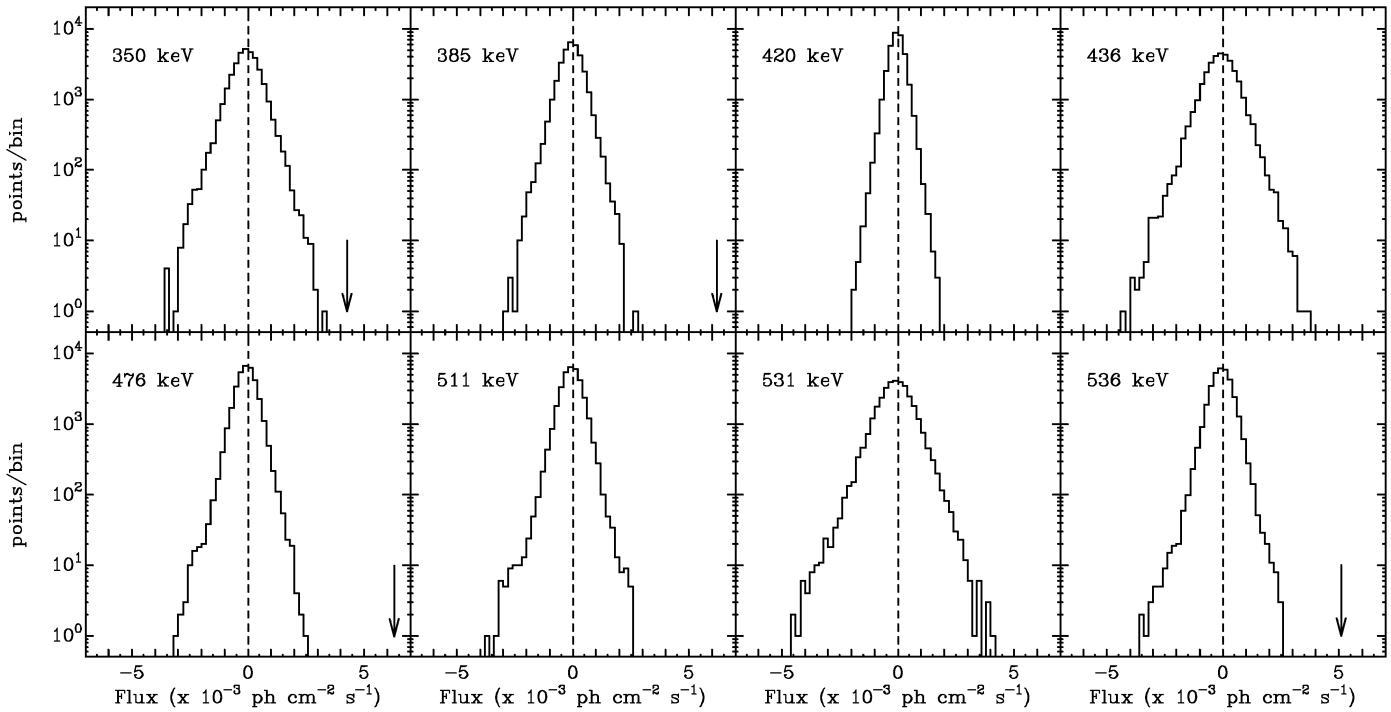

FIG. 5.—All-sky histograms of line fluxes for the eight lines of Table 2 for 1 day intervals. Where the line corresponds to a particular SIGMA transient, the SIGMA flux is shown by an arrow. Intervals starting at both 0 hr UT and 12 hr UT on each day for all 26 sky points are included. The histogram bins have width 0.2×10^{-3} photons s^{-1} cm^{-2}.

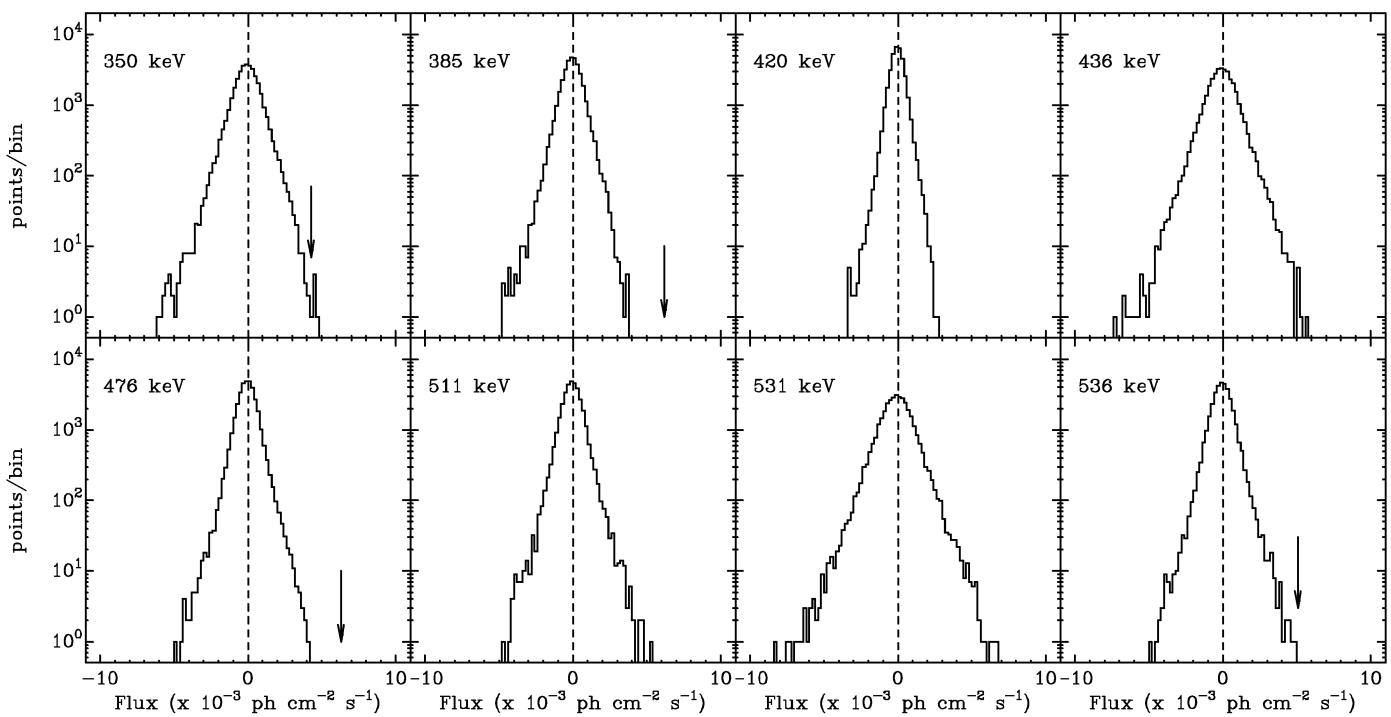

FIG. 6.—All-sky histograms for the eight lines of Table 2, 0.5 day intervals

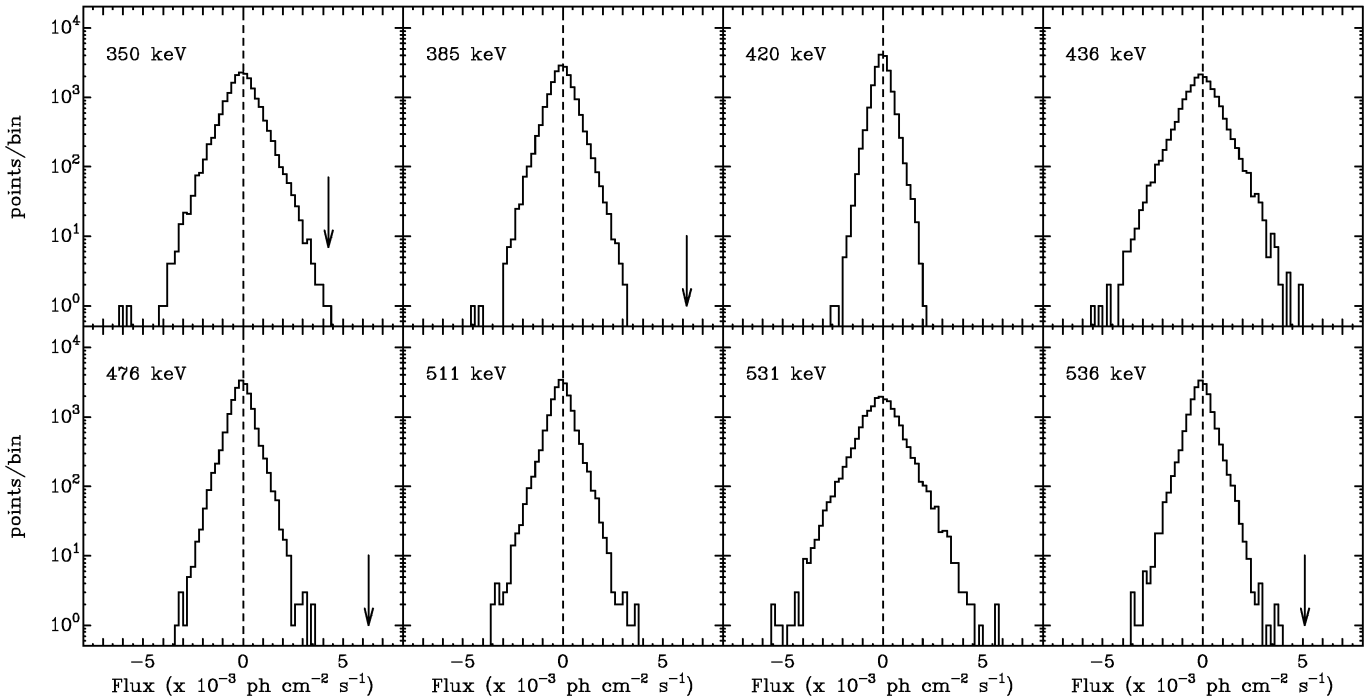

FIG. 7.—All-sky histograms for the eight lines of Table 2, 3 day intervals. Series starting on the first, second, and third days of data are included.

APPENDIX A

PARAMETERS FOR BACKGROUND EVALUATION

To decide whether a background spectrum is suitable, we evaluate parameters which affect the background and make sure the values are similar for the source and prospective background spectra. The threshold differences in each parameter have been determined empirically by examining large amounts of data, finding which parameters predict the background most effectively, eliminating those parameters which had little predictive power, and adjusting the overall tightness of the thresholds so that not more than 25% of the source spectra have to be eliminated. The parameters currently in use are:

1. *The angle between Earth's center and the detector normal.*—Since the background from the atmosphere is much harder than the diffuse background from the sky, this is the single most important parameter for determining the overall shape of the background spectrum.

2. *An empirical prediction of the atmospheric background generated from the BATSE data themselves.*—This parameter is a function of only the latitude and longitude of the spacecraft. The map of background level versus latitude and longitude was created by taking all BATSE spectra in 2 yr of data for which the Earth/detector angle (see above) was less than 45°. The LAD flux from 400–600 keV was averaged in 4° × 4° bins. The map, shown in Figure 8, looks very similar to models of geomagnetic cutoff rigidity. For a given spectrum, the parameter value is interpolated on the two-dimensional grid of the map; interpolation at 1° intervals was used for the figure.

3. *Number of seconds since the last SAA transit.*—This is used for orbits which have *not* included an SAA transit themselves. It is a crude measure of the activation background due to isotopes with half-lives greater than or on the order of an orbit.

4, 5. *Orbital phase since the ascending node, and longitude of the ascending node.*—When these two parameters are well matched, assuming the spacecraft orientation has not changed, the detectors' entire relation to Earth (including the first three parameters in this list) is approximately matched up.

6. *CPD count rate (for LADs) or Upper Level Discriminator (ULD) count rate (for SDs) for the detector of interest.*—These triggers count the rate of charged primary and secondary cosmic-ray particles. There are high energy (greater than tens of MeV) photons stopped in the SDs which trigger the ULD but at an insignificant rate compared to the cosmic-ray rate. When all the parameters involving geography and orientation are matched, these rates help determine the day-to-day variation in cosmic-ray bombardment which produces atmospheric, spacecraft, and detector background. The ULD rates have to be corrected for an empirically determined dependence on detector gain.

7. *The sum of the CPD or ULD rates for all eight detectors.*

8. *The A_p index of geomagnetic activity.*—We have found that the high-energy background drops significantly during times of high geomagnetic activity.

9. *The LAD count rate above 1 MeV (used for LADs only).*—In our last paper (Smith et al. 1996) we showed that it would take a very high MeV flux accompanying a 0.5 MeV transient to affect this parameter in a way that would bias our results because the LAD efficiency is already dropping rapidly by 0.5 MeV. In that paper, we used the SD data above 1 MeV to put strong limits on MeV emission at the time of the SIGMA transients from the Crab and from 1E 1740.7−2942 in 1992.

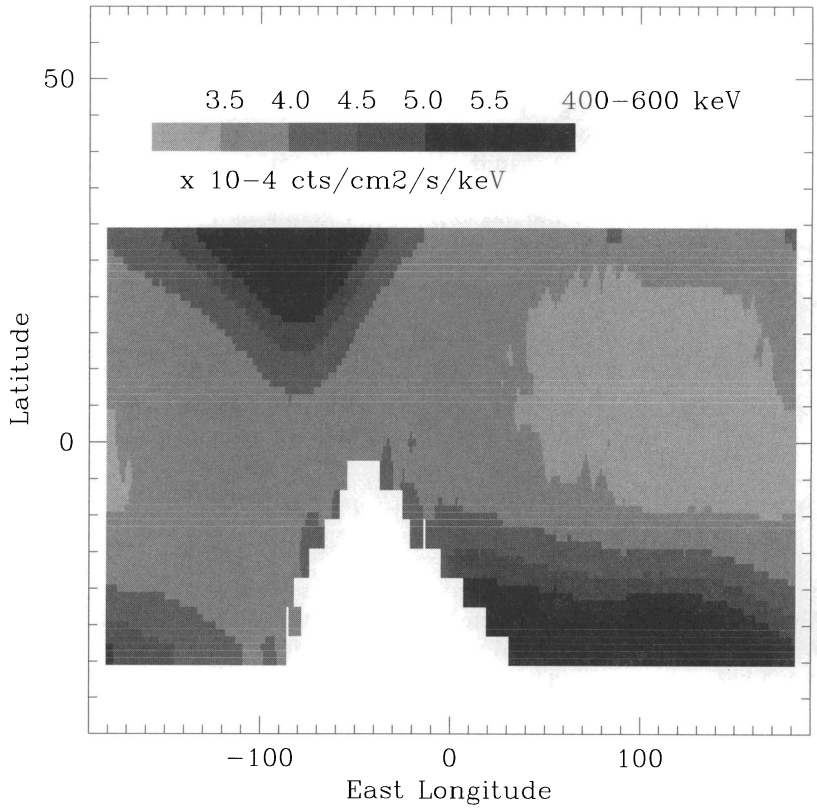

FIG. 8.—Empirical parameter consisting of the average downward-looking background from 400 to 600 keV as a function of geographic coordinates. No data are available during transits of the South Atlantic Anomaly.

10. *A measure from OSSE of the activation due to SAA passages.*—Although BATSE is shut off during SAA transits and cannot directly measure the charged-particle dose, OSSE keeps a particle counter running. Where OSSE data are missing, we use a fitting procedure to reproduce the likely dose based on nearby data and the longitude of the ascending node of the orbit. The activation is assumed to take place instantaneously in the middle of the SAA transit, and is subsequently convolved with either the 25 minute half-life of ^{128}I or the 15 hr half-life of ^{24}Na; these are two of the most important background-producing species in NaI scintillators (e.g., Battersby et al. 1993). There are many other isotopes which contribute, and these will be to some extent predicted by either the ^{128}I or ^{24}Na parameter, depending on their half-lives.

11. *The dot product of the detector normal with an eastward unit vector.*—Because of the east/west asymmetry in cosmic-ray bombardment, the ratio between charged particle count rates and photon background varies between eastward and westward detectors.

Sometimes a better match can be made for a source spectrum by interpolating between the chosen background spectrum and the spectrum closest to it in time. One hundred sets of parameters are generated by interpolating between the background spectrum and its neighbor in 1% increments, and the best match to the source spectrum is found; the background spectrum itself is then interpolated by the same amount.

APPENDIX B

TEMPLATES FOR BACKGROUND CORRECTION

We generate templates for background correction in three ways: each uses the values of a parameter in a trial set of many pairs of spectra and expresses how the spectra differ with a small change in the parameter. The type 1 template is conceptually the simplest, and we discuss it first for illustration; it is not used in the analysis. The template $T(E)$ is the average spectral difference at energy E per unit difference in parameter:

$$T(E) = \overline{\left[\frac{F_S(E) - F_B(E)}{P_S - P_B}\right]}, \tag{2}$$

where $F_S(E)$ and $F_B(E)$ are the source and background flux and P_S and P_B are the source and background values of the parameter. The average is over all the years of data available for a given detector, regardless of where in the sky it is pointing. Given a *particular* source and background spectrum to subtract during data analysis, we then use this template by replacing the background flux $F_B(E)$ with a corrected version:

$$F_B(E) \Leftarrow F_B(E) + T(E)(P_S - P_B)\,. \tag{3}$$

Figure 9 shows type 1 templates corresponding to two parameters. The first is the differential LAD spectrum corresponding to a small extra amount of CPD rate (parameter 6 above). The second is for a small amount of extra ^{128}I activation (parameter 10). Note that the latter shows a much stronger signal in the 511 keV positron-annihilation line. Each of these templates uses data where the Earth/detector angle (parameter 1) is between 80° and 100°. In fact, all the templates we use are actually sets of nine subtemplates, divided by 20° increments in this angle. This improves the predictive power of the templates, since different background components can dominate as this angle changes. For a given source and background pair, we interpolate between subtemplates using the average of the Earth angles for the source and background spectra.

In practice, more complicated forms for the templates work better than type 1. The type 2 template is the mean *percentage* difference in the source and background spectra per unit difference in the parameter:

$$T(E) = \overline{\left[\frac{F_S(E) - F_B(E)}{F_B(E)} \middle/ P_S - P_B \right]}, \tag{4}$$

and is applied by replacing $F_B(E)$ with

$$F_B(E) \Leftarrow F_B(E)[1 + T(E)(P_S - P_B)] - \frac{T(E)}{2}\,[F_B(E)(P_S - P_B) + F_S^*(E)(P_B - P_S)]\,. \tag{5}$$

The second term is a second-order correction which remedies a basic asymmetry: the background flux $F_B(E)$ appears in the first-order correction term but the source flux $F_S(E)$ cannot because we want the background we use to be independent of the source spectrum below 1 MeV. If $F_S^*(E)$ were set equal to $F_S(E)$, then this correction would assure that if the roles of source and background were reversed between two spectra, the subtracted spectrum would be equal in magnitude and opposite in sign. Without it, there is a small systematic negative bias to each subtraction which is only visible over large stretches of data. Since we refuse to use $F_S(E)$ in determining background, we instead substitute our best first-order guess at $F_S(E)$:

$$F_S^*(E) = F_B(E)[1 + T(E)(P_S - P_B)]\,. \tag{6}$$

Finally, the type 3 template is the mean percentage difference in the spectra per unit percentage difference in the parameter:

$$T(E) = \overline{\left[\frac{F_S(E) - F_B(E)}{F_B(E)} \middle/ \frac{P_S - P_B}{P_B} \right]}, \tag{7}$$

and is applied by replacing $F_B(E)$ with

$$F_B(E) \Leftarrow F_B(E)\left[1 + T(E)\,\frac{P_S - P_B}{P_B}\right] - \frac{T(E)}{2}\left[F_B(E)\,\frac{P_S - P_B}{P_B} + F_S^*(E)\,\frac{P_B - P_S}{P_S}\right], \tag{8}$$

with the best estimate of $F_S(E)$ for the second-order correction being

$$F_S^*(E) = F_B(E)\left[1 + T(E)\,\frac{P_S - P_B}{P_B}\right]. \tag{9}$$

For the LAD results presented here, we use a sequence of three template corrections: a type 3 template using the greater than 1 MeV LAD continuum (parameter 9), a type 3 template using the ratio of this continuum to the CPD rate (parameter 6), and a type 2 template using the SAA activation of ^{128}I (parameter 10). When using multiple templates, all previous templates must be applied while a new one is being generated so as to avoid duplicate corrections resulting from correlations between the parameters. Then the multiple templates may be applied in the same order when doing an analysis of a cosmic source. Figure 10 shows the three templates used for this analysis for the same range of Earth angle as was used for Figure 9. The depression near 511 keV in the second template and the negative values at other energies in the third template indicate that the first template often overcorrects when used alone. While generating each template, we calculate correlations between the remaining (source-background) residuals and a large number of parameters; this suggests which parameter to base the next template on.

Other templates have been examined but have little effect. For example, the template for SAA activation with the half-life of ^{24}Na shows a distinct peak near 200 keV, but we did not use this template because it seldom made much difference in the final results at higher energies. The extreme points for the lowest energy lines in Figure 7 are an exception and are discussed in the main text. The template types to be used, like the template parameters to be used, were determined by trial and error using large amounts of data either from the Galactic poles or taken randomly over the sky.

For the SDs, we use only two templates: a type 3 template using the ULD rate (parameter 6) and a type 2 template for SAA activation of ^{128}I (parameter 10). Because the SDs are smaller detectors than the LADs, it is easier to bring the residual systematic error close to the level of statistical errors in a day's data.

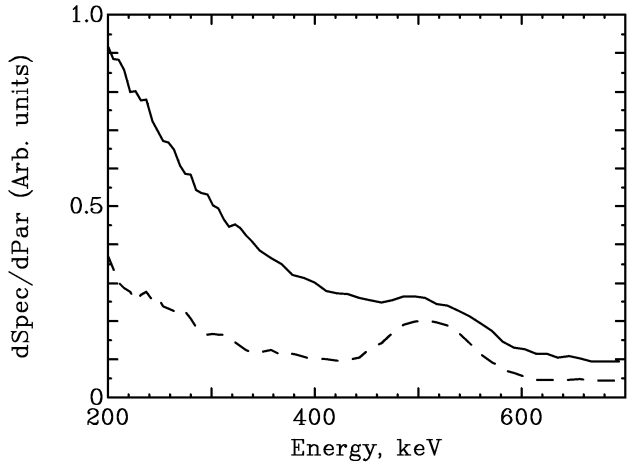

FIG. 9.—Type 1 template spectra representing the average incremental background per increment of increase in two parameters. *Dotted line:* activation from the last SAA pass convolved with the ^{128}I decay time. *Solid line:* CPD rate (i.e., prompt cosmic-ray dose). These templates are for Earth angles from 80° to 100° from the detector axis.

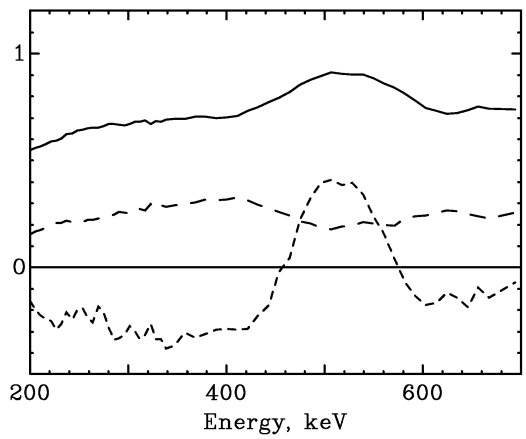

FIG. 10.—Templates used in the analysis. *Solid line:* type 3 template based on the greater than 1 MeV LAD rate. *Long dashes:* type 3 template based on the ratio of the CPD rate and greater than 1 MeV LAD rate with the first template already applied. *Short dashes:* type 2 template for ^{128}I activation from the SAA, with the first two already applied. Since the units of a type 2 template are different from those of a type 3 this trace has been arbitrarily rescaled to fit on the figure.

REFERENCES

Bally, J., & Leventhal, M. 1991, Nature, 353, 234
Battersby, S. J. R., et al. 1993, in Proc. Compton Gamma-Ray Observatory, ed. M. Friedlander, N. Gehrels, & D. J. Macomb (New York: AIP), 1107
Briggs, M., et al. 1995, ApJ, 442, 638
Chen, W., Gehrels, N., & Leventhal, M. 1994, ApJ, 426, 586
Churazov, E., et al. 1993, ApJ, 407, 753
Cordier, B., et al. 1993, A&A, 275, L1
———. 1994, in Proc. Second Compton Symp., ed. C. E. Fichtel, N. Gehrels, & J. P. Norris (New York: AIP), 446
Fishman, G., et al. 1989, in Proc. *GRO* Science Workshop, ed. W. N. Johnson (Washington, DC: NASA), 2-39
Gehrels, N., et al. 1991, ApJ, 375, L13
Gilfanov, M., et al. 1993, A&AS, 97, 303
———. 1994, ApJS, 92, 411
Goldwurm, A., et al. 1992, ApJ, 389, L79
Harmon, B. A., et al. 1994, in Proc. Second Compton Symp., ed. C. E. Fichtel, N. Gehrels, & J. P. Norris (New York: AIP), 210
Harris, M. J., Share, G. H., & Leising, M. D. 1994a, ApJ, 420, 649
———. 1994b, ApJ, 433, 87
Heindl, W., et al. 1993, ApJ, 408, 503
———. 1994, ApJ, 430, 829
Hjellming, R. M., & Rupen, M. P. 1995, Nature, 375, 464
Hua, X., & Lingenfelter, R. E. 1993, ApJ, 416, L17
Jung, G. V., et al. 1995, A&A, 295, L23
Leventhal, M., et al. 1993, ApJ, 405, L25
Lingenfelter, R. E., & Ramaty, R. 1989, ApJ, 343, 686
Lund, N. 1993, A&AS, 97, 289
Maciołek-Niedźwiecki, A., & Zdziarski, A. A. 1994, ApJ, 436, 762
Mirabel, I. F., et al. 1991, A&A, 251, L43
Mirabel, I. F. 1992, Nature, 358, 215
Mirabel, I. F., & Rodriguez, L. 1994, Nature, 371, 46
Misra, R., & Melia, F. 1993, ApJ, 419, L25
Orosz, J. A., et al. 1994, ApJ, 436, 848
Owens, A. 1991, in Gamma-Ray Line Astrophysics, ed. P. Durouchoux & N. Prantzos (New York: AIP), 341
Purcell, W. R., et al. 1993, ApJ, 413, L85
Ramaty, R., Leventhal, M., Chan, K. W., & Lingenfelter, R. E. 1992, ApJ, 392, L63
Rodriguez, L. F., et al. 1992, ApJ, 401, L15
Share, G. H., et al. 1990, ApJ, 358, L45
Skibo, J. G., Dermer, C. D., & Ramaty, R. 1994, ApJ, 431, L39
Smith, D. M., et al. 1993, ApJ, 414, 165
———. 1996, ApJ, 458, 576
Sunyaev, R., et al. 1991, ApJ, 383, L49
———. 1992, ApJ, 389, L75
Tueller, J., et al. 1996, A&AS, in press
Wallyn, P., et al. 1996, A&AS, in press